Purification and functional characterization of the vacuolar malate transporter tDT from *Arabidopsis*

Received for publication, November 7, 2017, and in revised form, January 8, 2018 Published, Papers in Press, January 24, 2018, DOI 10.1074/jbc.RA117.000851

Benedikt Frei[‡], Cornelia Eisenach[§], Enrico Martinoia[§], Shaimaa Hussein[¶], Xing-Zhen Chen[¶], Stéphanie Arrivault[‖], and H. Ekkehard Neuhaus[‡1]

From [‡]Pflanzenphysiologie, Universität Kaiserslautern, Erwin Schrödinger-Strasse, D-67653 Kaiserslautern, Germany, the [§]Institut für Pflanzenbiologie, Universität Zürich, CH-8008 Zürich, Switzerland, the [¶]Faculty of Medicine and Dentistry, Department of Physiology, University of Alberta, Edmonton, Alberta T6G 2H7, Canada, and the [‖]Max Planck-Institute of Molecular Plant Physiology, Wissenschaftspark Potsdam-Golm, Am Mühlenberg 1, D-14476 Potsdam, Germany

Edited by Joseph M. Jez

The exact transport characteristics of the vacuolar dicarboxylate transporter tDT from *Arabidopsis* are elusive. To overcome this limitation, we combined a range of experimental approaches comprising generation/analysis of *tDT* overexpressors, $^{13}CO_2$ feeding and quantification of ^{13}C enrichment, functional characterization of tDT in proteoliposomes, and electrophysiological studies on vacuoles. *tdt* knockout plants showed decreased malate and increased citrate concentrations in leaves during the diurnal light-dark rhythm and after onset of drought, when compared with wildtypes. Interestingly, under the latter two conditions, *tDT* overexpressors exhibited malate and citrate levels opposite to *tdt* knockout plants. Highly purified tDT protein transports malate and citrate in a 1:1 antiport mode. The apparent affinity for malate decreased with decreasing pH, whereas citrate affinity increased. This observation indicates that tDT exhibits a preference for dianion substrates, which is supported by electrophysiological analysis on intact vacuoles. tDT also accepts fumarate and succinate as substrates, but not α-ketoglutarate, gluconate, sulfate, or phosphate. Taking tDT as an example, we demonstrated that it is possible to reconstitute a vacuolar metabolite transporter functionally in proteoliposomes. The displayed, so far unknown counterexchange properties of tDT now explain the frequently observed reciprocal concentration changes of malate and citrate in leaves from various plant species. tDT from *Arabidopsis* is the first member of the well-known and widely present SLC13 group of carrier proteins, exhibiting an antiport mode of transport.

Carboxylates, such as malate, citrate, and fumarate, are major constituents of cellular processes in virtually every living system. In plants, these compounds are involved in several important metabolic pathways and serve as intermediates of energy metabolism; as precursors for metabolites, such as amino acids, sugars, and nucleotides; as chelators for metallic nutrients and toxic heavy metals; as counterions for cations; as solutes required for regulation of cell turgor; or as signal molecules (1–4). Malate, as a majorly abundant carboxylate, possesses two pK_a values of pH 3.1 and 5.1, respectively, which makes this solute, moreover, a critical element of the "pH-stat system" in plant cells (5). Malate is known as an intermediate of mitochondrial metabolism, but it is also found in the cytosol, chloroplasts, peroxisomes, vacuoles, and apoplast (6). Thus, the presence of malate in most cellular domains and its central function in many biochemical pathways require a tightly controlled homeostasis.

The vacuole serves as a buffer and storage compartment for malate, which allows this metabolite to be provided under selected conditions, thus keeping cytosolic concentrations at an optimum (7). However, because leaf malate contents exhibit a marked diurnal fluctuation (8), vacuolar storage must be a dynamic process. Accordingly, the regulation of import and export of malate is necessary to adjust its cellular availability to changing cellular demands.

Malate transport across the vacuolar membrane is mediated by different transport systems, allowing this organic acid to accumulate even against steep concentration gradients (7). Direct uptake experiments and electrophysiological studies on either tonoplast-enriched vesicles or intact vacuoles from different plant species indicate the presence of both malate carriers and rectifying malate channel proteins (9–14).

The tonoplast dicarboxylate transporter (tDT)[2] from *Arabidopsis* was the first vacuolar malate carrier identified at the molecular level (8). In *Arabidopsis*, no homologs of the *tDT* gene exist, and the presence of this carrier is most likely limited to the vacuolar membrane (8) and plant tDT protein group in the so-called SLC13 family. In contrast to tDT, all SLC13 proteins in animal cells reside on the plasma membrane and catalyze sodium-coupled import of various carboxylates (15, 16).

Vacuolar malate uptake by tDT might be partially complemented by the tonoplast-located membrane protein ALMT9, found in *Arabidopsis* (11, 17). The latter is a member of the

This work was supported by the Deutsche Forschungsgemeinschaft (DFG) in the framework of the International Research Training Group 1830 (IRTG 1830). The authors declare that they have no conflicts of interest with the contents of this article.

This article contains Figs. S1–S3.

[1] To whom correspondence should be addressed: Universität Kaiserslautern, Erwin Schrödinger-Str., D-67653 Kaiserslautern, Germany. Tel.: 49-631-2052372; Fax: 49-631-2052600; E-mail: neuhaus@rhrk.uni-kl.de.

[2] The abbreviations used are: tDT, tonoplast dicarboxylate transporter; gFw, grams formula weight; oex, overexpressor; DDM, dodecyl maltoside; Ni-NTA, nickel-nitrilotriaceticacid; Tricine, *N*-[2-hydroxy-1,1-bis(hydroxymethyl)ethyl]glycine; BisTris propane, 1,3-bis[tris(hydroxymethyl)methylamino] propane; IMAC, immobilized metal-ion chromatography.

aluminum-activated malate transporter family, because the first members of this protein group have been identified in the plasma membrane from root cells, where they contribute to the extraradical chelation of toxic aluminum (18). Electrophysiological studies demonstrated that ALMT9 accepts, as a channel-type protein, both malate and fumarate as substrates and exhibits inward-rectifying carboxylate currents (11). More detailed studies showed that ALMT9 is likely to function also as a malate-activated chloride channel and that its physiological role is probably vacuolar Cl^- uptake (19, 20), and in a recent publication it was revealed that an ALMT member in tomato fulfills a central role in fruit malate accumulation (17).

Surprisingly, compared with wildtype plants, tDT loss-of-function mutants from *Arabidopsis* did not exhibit morphological alterations or developmental retardation or impaired stomata movement when exposed to different growth conditions (21). However, the mutant showed metabolic alterations clearly pointing to an *in vivo* malate transport activity. These differences include decreased leaf malate levels, increased respiration, an altered respiratory coefficient, and changes in mitochondrial metabolites. Furthermore, mutant plants were impaired in their ability to cope with acid stress (8, 21–23). These results suggest that vacuolar ALMTs can partially compensate for the loss of tDT and that corresponding mutants can adapt their metabolism to a situation where malate is less efficiently transferred to the vacuole mainly by increasing consumption of malate.

To further describe the physiological impact of tDT on plant malate homeostasis and to identify the so far unresolved mode of transport catalyzed by tDT, we used a range of experimental approaches. After considering all data obtained, we describe a so far unknown malate/citrate antiport catalyzed by tDT, atypical of all other SLC13 proteins analyzed so far. This unexpected transport property of tDT allows us now to explain the frequently observed cellular carboxylate homeostasis in higher plants.

Results

Generation of tDT overexpressor lines

In a previous publication (8), two independent tDT knockout lines (abbreviated as *tdt1* and *-2*) have been described, which both exhibit similar physiological and metabolic differences when compared with wildtypes.

For the present study, we wanted to additionally generate *tDT* overexpressor mutants (oex lines). For this purpose, the *tDT* cDNA from *Arabidopsis* was set under control of the 35S-cauliflower mosaic virus promoter. To prevent a putative co-suppression, the artificial *tDT* gene was introduced into the genetic background of the knockout line *tdt1* (8). From 10 independent *tDT* oex lines, we isolated total mRNA and conducted Northern blot analysis. All oex lines selected exhibited a substantial accumulation of *tDT* transcripts (Fig. S1*A*). oex lines 15 and 24 (*marked*) were analyzed by quantitative RT-PCR and showed 60- and 40-fold increased *tDT* mRNA levels, respectively, when compared with the *tDT* mRNA content present in WT (Fig. S1*B*).

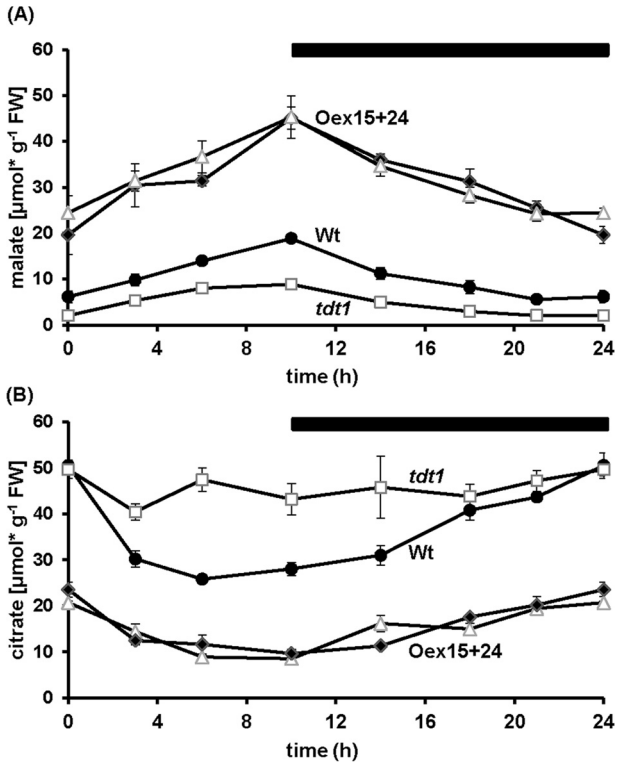

Figure 1. Malate and citrate contents in *Arabidopsis* leaves. Shown are malate (*A*) and citrate (*B*) contents in plants from wildtype (*black circles*), *tDt1* (*white squares*), and *tDT* overexpressor plants oex15 (*white triangles*) and oex24 (*black diamonds*). Plants were grown under standard conditions for 5 weeks. Samples were harvested in a diurnal rhythm at the given time points. *Black bars*, periods of darkness. Each *data point* represents the mean value of four biological replicates ± S.E. (*error bars*).

tDT overexpressors and tDT knockout plants exhibit reciprocal diurnal malate and citrate levels

To analyze the effect of altered tDT activity on carboxylate contents, we grew WT plants, the mutants *oex15* and *oex24*, and *tdt1* plants for 5 weeks on soil and quantified leaf carboxylate levels in the course of a day/night cycle (10 h of light and 14 h of darkness; Fig. 1, *A* and *B*).

WT plants contained 6.2 μmol of malate/gFw at the end of the night and accumulated this organic acid linearly over the entire light phase, reaching 18.8 μmol of malate/gFw (Fig. 1*A*). In the following dark period, the malate concentration decreased and reached, after 14 h of darkness, a value similar to light onset (Fig. 1*A*). *tdt1* plants contained only 2.0 μmol of malate/gFw at the end of the night and accumulate only 8.9 μmol of malate/gFw at the end of the day, which corresponds to ~50% of the value observed for the WT (Fig. 1*A*). During the night phase, malate in *tdt1* leaves decreased to a value similar to the concentration at the start of illumination (Fig. 1*A*). In marked contrast, both *tDT* oex lines contained significantly increased malate levels when compared with the other two genotypes. At the end of the night phase, oex15 and oex24 contained 19.6 and 24.4 μmol of malate/gFw, respectively, and accumulated malate linearly over the entire day phase, reaching in both lines 45.3 μmol of malate/gFw (Fig. 1*A*). Similar to the other genotypes, malate levels decreased in a nearly linear fashion during the night and reached 20 and 24 μmol/gFw in oex15 and oex24 leaves, respectively (Fig. 1*A*).

In wildtypes, the diurnal levels of citrate behaved reciprocally to the changes in malate during the entire day. WT plants contained about 50 μmol/gFw citrate at the beginning of the light phase, and this content decreased rapidly during the first 3 h of light, approaching 30.2 μmol/gFw (Fig. 1*B*). Subsequent to this, citrate levels decreased further, leading to a concentration of 28.0 μmol/gFw at the end of the light phase (Fig. 1*A*). During the night, the citrate concentration increased and reached a level close to the value present at the beginning of the experiment, namely 50.5 μmol/gFw (Fig. 1*A*). In contrast to this, changes in citrate in the *tdt1* were much less pronounced (Fig. 1*B*). At the beginning of the light phase, *tdt1* plants contained citrate levels resembling the value present in WT leaves, whereas citrate consumption during the day was marginal, leading to 43.1 μmol of citrate/gFw (Fig. 1*B*). This citrate level increased only slightly within the 14 h of darkness and reached a value of about 50 μmol/gFw, which is similar to that at the start of the analysis (Fig. 1*B*). In strong contrast to the situation in WT or *tdt1* plants, leaves from the two *tDT* oex lines 15 and 24 contained much less citrate. oex lines 15 and 24 started with 20.6 and 23.5 μmol of citrate/gFw, respectively, at the beginning of the light phase, and this low concentration decreased further during the day, leading to only 10 μmol of citrate/gFw in both plant lines (Fig. 1*B*). During the following night phase, citrate in both oex lines increased nearly linearly and reached values close to those at the start of the analysis (Fig. 1*B*).

In general, onset of drought stress provokes increased levels of carboxylic acids in plants (24). Thus, to reveal whether the differences in carboxylate contents between the individual genotypes are limited to a diurnal dynamic, we additionally checked the effect of drought on these metabolites. For this, we grew all plant lines for 3 weeks on soil before the onset of drought, induced by withdrawing of water for 14 days, whereas the controls were further watered. At the end of the light phase of the 14 days of drought stress, samples were taken, and carboxylates were quantified. In WT plants, drought provoked a substantial increase of the leaf malate concentration from 15.1 μmol/gFw in watered plants to 45.5 μmol/gFw. In the *tdt1* line, almost no drought-induced increase in malate content was observed, whereas both *tDT* overexpressor lines started already with higher malate levels when compared with WT, namely 41.6 and 31.0 μmol of malate/gFw, respectively (Fig. 2*A*). By contrast, in WT plants drought provoked a decrease of citrate, because watered WT leaves contained 22.4 μmol of citrate/gFw, whereas drought exposure led to less than 10 μmol of citrate/gFw (Fig. 2*B*). Loss-of-function *tdt1* plants contained higher citrate levels than corresponding WT plants (about 43.3 μmol of citrate/gFw in controls), and, similar to malate changes, drought-induced changes in citrate were not significant in this plant genotype (Fig. 2*B*). Both *tDT* overexpressor lines contained significantly less citrate than WT or *tdt1* plants under both control and drought conditions (Fig. 2*B*). The low citrate levels in oex mutants, only about 10 μmol of citrate/gFw, were not substantially reduced by drought treatment, indicating that in this case, only a moderate correlation could be observed between the inverse malate and citrate concentrations (Fig. 2*B*). This result is probably due to the fact that citrate

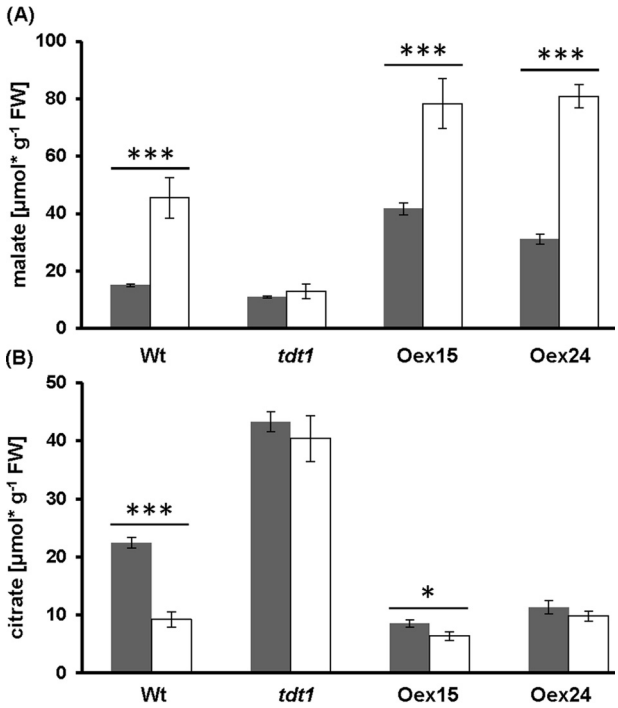

Figure 2. Changes in citrate and malate contents in *Arabidopsis* leaves after 14 days of drought. WT, knockout (*tdt1*), and *tDT* overexpressor plants (*Oex15* and *Oex24*) were grown under standard conditions for 3 weeks. Subsequent to this, drought was applied by withholding water for 14 days (*white*). *A*, malate levels; *B*, citrate levels. Control plants were still watered (*dark gray*). Samples were harvested at the end of the dark period. Each *data point* represents the mean value of 14 biological replicates ± S.E. (*error bars*). *Asterisks* indicate statistically significant differences analyzed with Student's *t* test (*, $p \leq 0.05$; **, $p \leq 0.01$; ***, $p \leq 0.001$).

detected in oex plants is mostly cytosolic, and hence no further substantial decrease could be observed.

tDT shows marked pH dependence of carboxylate transport

Proteoliposomes, containing a pure carrier protein, represent an excellent tool to study general transport properties. However, so far there has been no report on reconstitution of a purified vacuolar metabolite transporter in liposomes. Thus, a suitable reconstitution protocol is missing.

To this end, we expressed tDT heterologously in *Escherichia coli* and reconstituted the purified recombinant tDT protein in liposomes, which additionally allowed us to define luminal solute composition. After recombinant synthesis of a His-tagged tDT protein (His-tDT), we enriched the fusion protein by use of a metal-chelate affinity chromatography, leading to a purified carrier exhibiting an apparent molecular mass of about 50 kDa (Fig. S2*A*). Using a His tag–specific antibody, we confirmed that the size of the purified protein (Fig. S2*A*) corresponds to the recombinant transporter (Fig. S2*B*).

Liposomes, containing the reconstituted His-tDT protein (most likely reconstituted in the 1:1 orientation), imported both citrate and malate, and transport of both metabolites was stimulated by preloading of vesicles with either malate or citrate (Fig. 3*A*). At an external pH of 7.8, [^{14}C]malate import into preloaded proteoliposomes was maximal (Fig. 3*A*, *left*), whereas decreasing the external pH to either 7.0 or 6.2 provoked a stepwise lowered transport rate (Fig. 3*A*, *middle* and *right*). Similar to malate uptake,

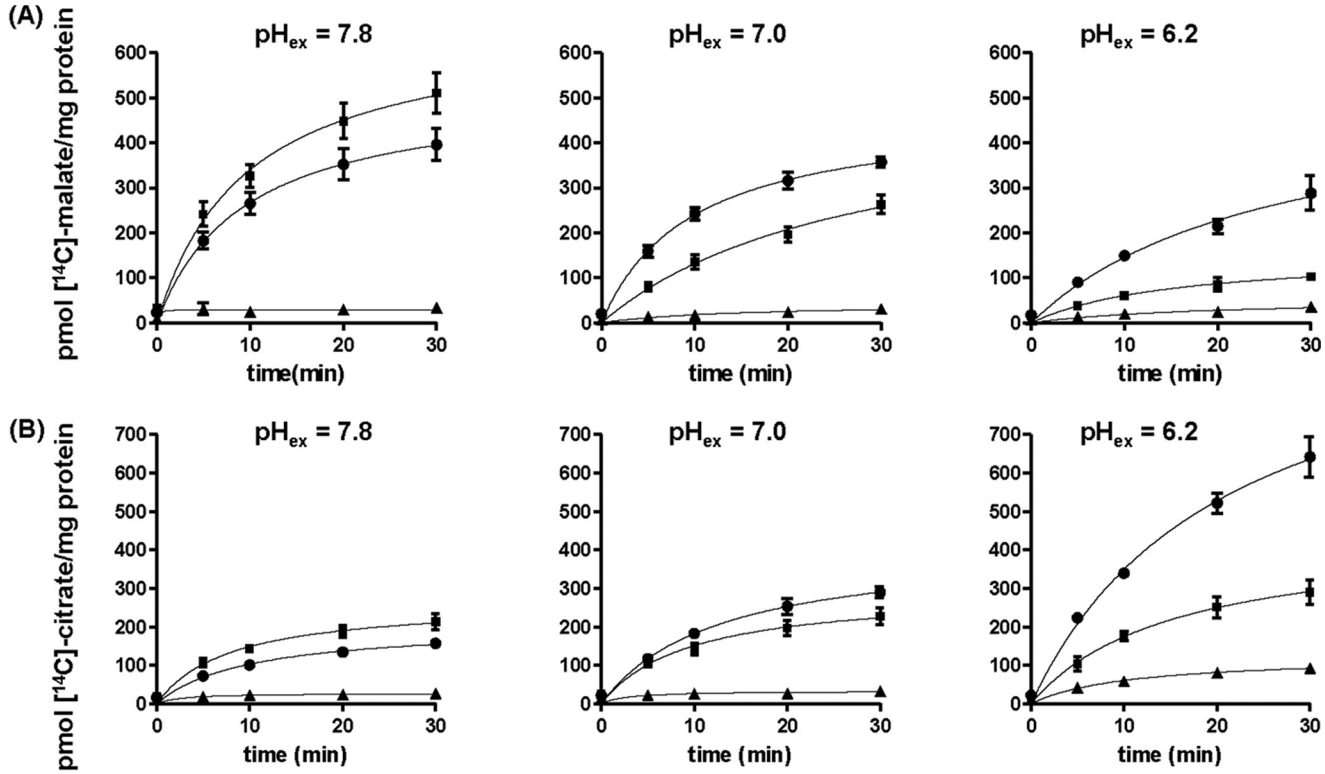

Figure 3. Time dependence of tDT-mediated malate and citrate uptake into proteoliposomes. Proteoliposomes were incubated with either 50 μM ^{14}C-labeled citrate or malate, respectively, for the indicated time. Concentration of preloaded carboxylates was 5 mM. Uptake was stopped by separation of external carboxylates from proteoliposomes by anion-exchange chromatography. *A*, time dependence of malate uptake into malate-loaded (*circles*), citrate-loaded (*squares*), or unloaded proteoliposomes (*triangles*). *B*, time dependence of citrate uptake into malate-loaded (*circles*), citrate-loaded (*squares*), or unloaded proteoliposomes (*triangles*). Luminal pH was always set to 7. Each *data point* represents the mean value of at least five independent experiments ± S.E. (*error bars*).

rates of tDT-mediated citrate uptake were extremely low in unloaded proteoliposomes (tgl medium; lacking additional carboxylates; Fig. 3*B*). However, preloading of proteoliposomes with either citrate or malate substantially stimulated [^{14}C]citrate uptake (Fig. 3*B*, *left*). In opposition to malate transport, citrate transport by tDT was slightly increased by decreasing the external pH from 7.8 to 7 (Fig. 3*B*, *middle*) and was strongly stimulated by further acidification to pH 6.2 (Fig. 3*B*, *right panel*).

Alterations of external pH affect malate and citrate affinity of tDT in a reciprocal manner

To reveal whether the external pH affects substrate affinities, we conducted additional uptake experiments at changing external carboxylate concentrations and at various pH levels (Fig. 4, *A* and *B*). tDT-mediated malate import rates were lowered by external acidification from pH 7.8 to pH 6.2, resulting in decreased apparent substrate affinities ranging from about 200 μM at pH 7.8 to about 490 μM at pH 6.2 (Fig. 4*A* (*left* to *right panel*) and Table 1). In contrast, external acidification led to increased rates of citrate transport rates by the tDT protein and to higher apparent affinities for citrate ranging from K_m values 364 μM at pH 7.8 to 303 μM at pH 7 and 158 μM at pH 6.2 (Fig. 4 (*A* and *B*) and Table 1).

AttDT carrier accepts various carboxylic acids, performs carboxylate antiport, and prefers divalent charged carboxylates

To check whether tDT accepts substrates other than malate and citrate, we analyzed the relative efficiencies of preloading proteoliposomes with a range of putative solutes (Fig. 5) at pH 7.8 and 6.2. From all solutes tested, malate and citrate were most efficient as counterexchange substrates (Fig. 5, *A* and *B*). Similar to the observation above, malate uptake was higher at the alkaline pH of 7.8 when compared with the acidic pH of 6.2, whereas citrate uptakes behaved reciprocally (Fig. 5, *A* and *B*). Both malate and citrate uptakes were stimulated by preloading of the proteoliposomes with fumarate and succinate, whereas phosphate and sulfate did not serve as lumenally located, transport-stimulating solutes (Fig. 5, *A* and *B*). In addition, because unloaded proteoliposomes imported malate and succinate only at rates similar to phosphate- or sulfate-induced transport (Fig. 5, *A* and *B*), we conclude, in addition, that tDT does not accept gluconate (present at a concentration of 30 mM in tgl-buffer medium) as a substrate.

To gain information on whether the observed stimulatory effect of luminal carboxylates on tDT-mediated transport is through an antiport mechanism or by a trans-stimulation process (25), we conducted counterexchange experiments, similar to our previous experiments on the reconstituted ATP/ADP exchanger NTT from bacteria (26). To this end, we preloaded proteoliposomes with either non-radioactive or radioactively labeled malate (each at a concentration of 50 μM) and quantified the uptake of radioactive or non-radioactive citrate, respectively (Fig. 5*A*, *inset*). By comparison of export and import of radioactivity, we revealed a counterexchange transport mode at about 1:1 stoichiometry (Fig. 5*A*, *inset*).

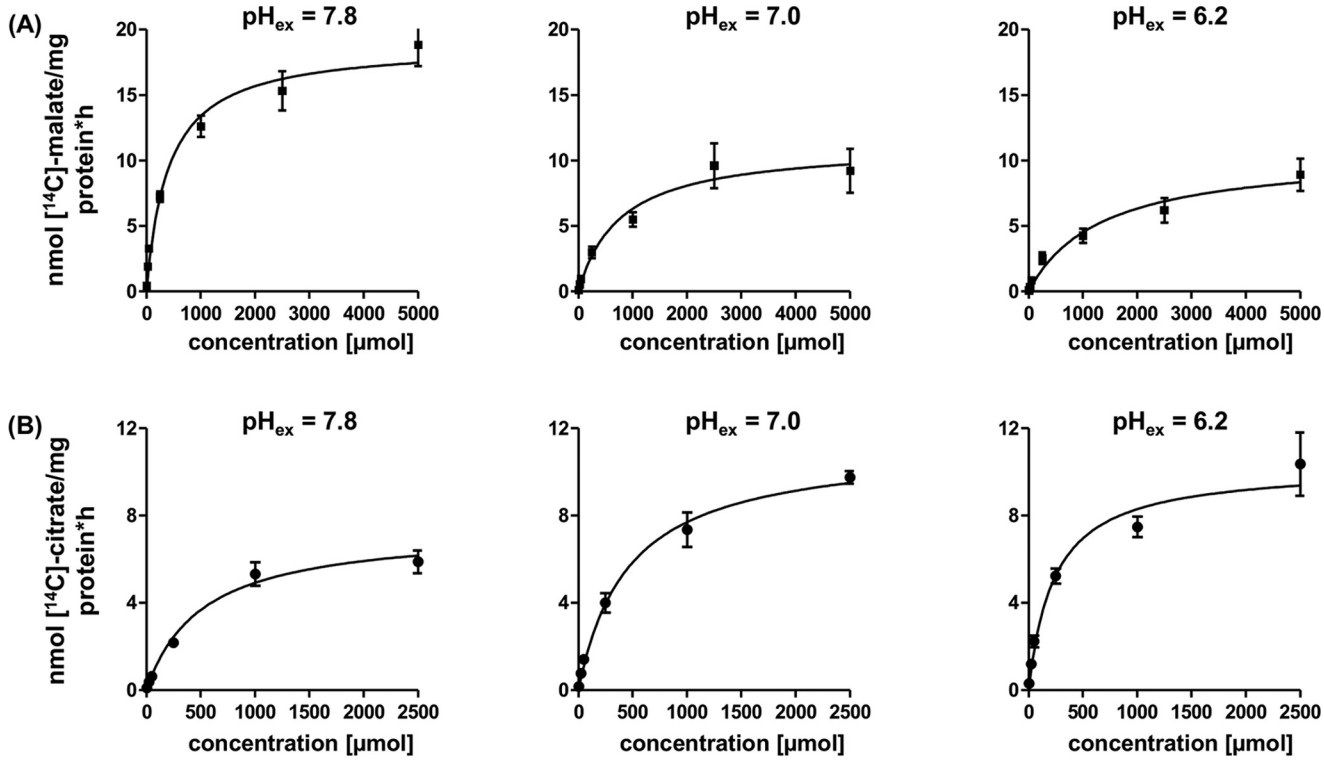

Figure 4. Concentration dependence of ^{14}C-labeled malate or citrate uptake into tDT-containing proteoliposomes. *A*, uptake of ^{14}C-labeled malate into proteoliposomes preloaded with 5 mM malate. *B*, uptake of ^{14}C-labeled citrate into proteoliposomes preloaded with 5 mM citrate. pH levels on the luminal site of the proteoliposomes were adjusted to pH 7.0. Substrates from the external site were supplied at pH ranging from alkaline (pH$_{ex}$ 7.8) to neutral (pH$_{ex}$ 7.0) to acidic (pH$_{ex}$ 6.2). Each *data point* represents the mean value of at least five individual replicates ± S.E. (*error bars*).

Table 1
Apparent K_m values and V_{max} values of malate and citrate import into preloaded tDT proteoliposomes

pH (external/internal)	Malate uptake (citrate preloaded)		Citrate uptake (malate preloaded)	
	K_m	V_{max}	K_m	V_{max}
	µM	*nmol/mg protein h*	µM	*nmol/mg protein h*
7.8/7.0	197.8 ± 12.59	16.2 ± 0.64	363.7 ± 30.51	6.2 ± 0.37
7.0/7.0	443.0 ± 46.20	9.5 ± 0.68	303.2 ± 16.69	9.8 ± 0.38
6.2/7.0	488.9 ± 46.76	7.7 ± 0.51	158.0 ± 10.37	9.2 ± 0.40

So far, the charge of the carboxylate substrate transported by tDT has been unknown. To fill this gap in knowledge, we conducted import studies directed at changing external pH and quantified citrate uptake at pH values ranging from 7 to 4 (Fig. 6). As expected, citrate uptake rates were lowest at neutral pH (3 nmol/mg protein h^{-1}) and increased with acidification of the medium. At pH 4.6, a maximal citrate uptake of about 60 nmol/mg protein h^{-1} was observed, which declined rapidly by a slight further acidification to pH 4, where only 33 nmol of citrate/mg of protein h^{-1} was imported (Fig. 6). This pH dependence of citrate transport correlates with the distribution of individual citrate anions in media of different pH (Fig. 6). The highest concentration of citrate^{2-} is present at pH 5.3 and decreased rapidly toward further acidification. At pH 4, only 15% of citrate is in its dianion (2−) form, and 78% is in its 1− form. These data led us to suggest that citrate^{2-} is the predominantly transported substrate.

To test the hypothesis that tDT exchanges divalent charged carboxylic acids, we conducted electrophysiological studies on isolated vacuoles from *tdt1* plants or from the oex line 15 (Fig. S3). Substrate-induced currents were measured in the so-called "whole-vacuole" configuration, allowing to measure fluxes across the total vacuolar surface. Vacuoles of *tdt* knockout and the representative overexpressor line 15 were measured in the presence of symmetric citrate concentrations initially, and the bath solution was subsequently switched to malate (Fig. S3, *A* and *B*). The presence of both putative substrates on either side of the membrane did not, however, change current density. *I*-V curves of current densities over a range of voltages did not differ, neither between *tdt1* and *oex15* nor between different substrates (Fig. S3*C*). The latter results indicate that the citrate/malate exchange, presumably ongoing across the tonoplast from overexpressor vacuoles, is not electrogenic.

Arabidopsis tDT mutants exhibit altered rates of carboxylic acid labeling from newly assimilated CO_2

The data above led us to assume that tDT mediates an exchange of malate and citrate across the vacuolar membrane. Accordingly, we also conducted $^{13}CO_2$ labeling of WT, *tdt1*, and *tDT* overexpressor rosette leaves under ambient steady-state conditions, which allows quantification of the incorporation of ^{13}C into compounds of the primary carbon metabolism

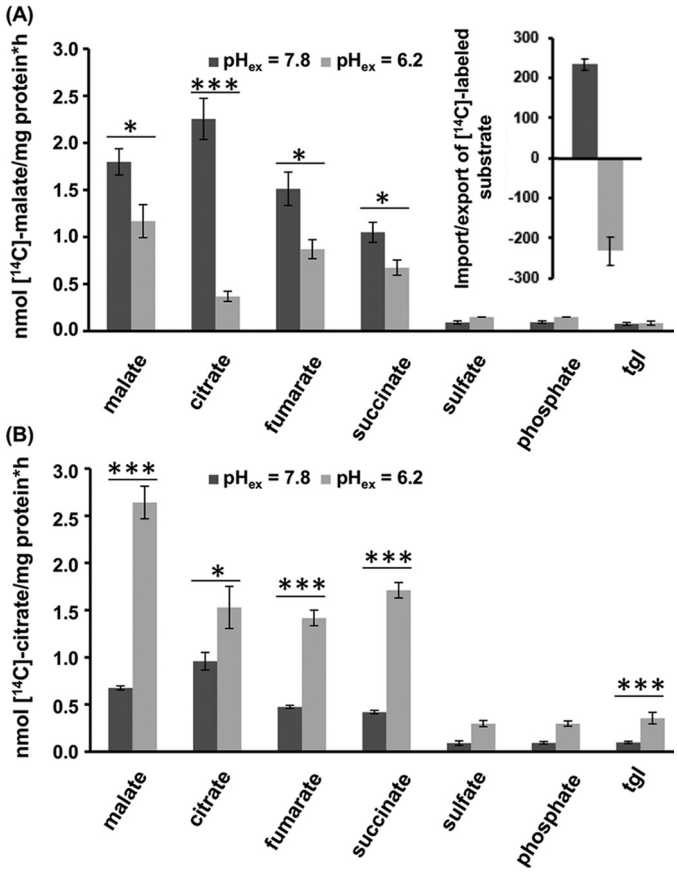

Figure 5. Influence of different internal substrates on ^{14}C-labeled malate or citrate import into tDT proteoliposomes and counterexchange stoichiometry. Proteoliposomes were incubated with 50 μM ^{14}C-labeled citrate or malate, respectively, and uptake was stopped after 5 min by separation of external carboxylates from proteoliposomes by anion-exchange chromatography. *A*, uptake of ^{14}C-labeled malate into preloaded proteoliposomes at external pH values of 7.8 (*dark gray*) or 6.2 (*light gray*). *Inset*, comparison of [^{14}C]citrate import *versus* [^{14}C]malate export. [^{14}C]Citrate (50 μM) import (*dark gray bar*) was measured on proteoliposomes preloaded with 50 μM unlabeled malate, and [^{14}C]malate export (50 μM luminal concentration; *light gray bar*) was measured at an external citrate concentration of 50 μM. Transport was allowed for 2 min and stopped by anion-exchange chromatography. Rates are given in pmol/mg protein. *B*, uptake of ^{14}C-labeled citrate into preloaded proteoliposomes at external pH values of 7.8 (*dark gray*) or 6.2 (*light gray*). Concentration of loaded substrates were 5 mM. Luminal pH was always set to 7. Each data point represents a mean value of at least five independent experiments ± S.E. (*error bars*). *Asterisks* indicate statistically significant differences analyzed with Student's *t* test (*, $p \leq 0.05$; **, $p \leq 0.01$; ***, $p \leq 0.001$).

(27), here with a particular interest in malate and citrate. Due to technical limitations, it was not possible to separate the isotopomers of citrate and isocitrate. However, no enrichment was observed in citrate/isocitrate even after 40 min of labeling. Therefore, only $^{13}CO_2$ incorporation into malate is presented here.

Considering that the malate pool size is smaller in *tdt1* mutants and higher in overexpressor lines when compared with WT (Figs. 1 and 2), we expected that ^{13}C labeling would be faster in *tdt1* mutants and slower in the selected oex plant. In fact, it could be observed that $^{13}CO_2$ incorporation into malate in *tdt1* mutants was faster than in WT plants, whereas in overexpressor line 15, malate was labeled with less efficiency than observed on WT plants (Fig. 7). This effect was already observed after 3 min and was more pronounced after 10, 20, and 40 min.

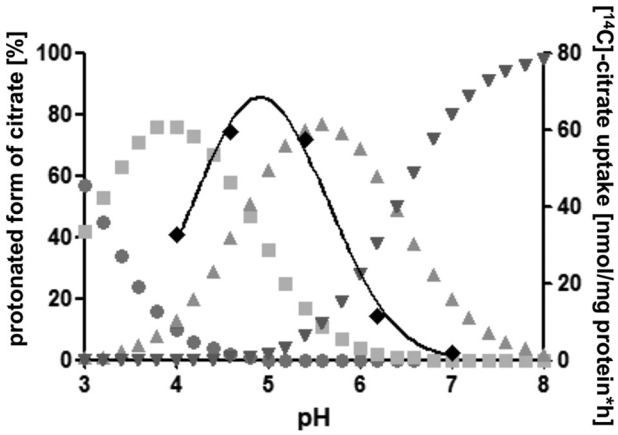

Figure 6. Uptake of ^{14}C-radioactively labeled citrate into proteoliposomes under different pH conditions and occurrence of different citrate ions dependent on pH. Citrate uptake into proteoliposomes preloaded with 50 μM malate (*black diamonds*) was compared with the distribution of citrate ions at different pH conditions. pH on the luminal site of the proteoliposomes was adjusted to pH 7.0. Uptake of ^{14}C-labeled citrate was quantified at different pH values, ranging from 4.0 to 7.0. Each data point represents the mean value of three individual replicates ± S.E. Calculation of citrate ion distribution was done using CurTiPot–pH and acid–base titration curves: Analysis and Simulation software, version 4.2.0: citrate H_3 (*red circles*), citrate^{1-} H_2 (*yellow squares*), citrate^{2-} H (*blue triangles*), citrate^{3-} (*purple triangles*).

Discussion

AttDT activity limits vacuolar malate accumulation in Arabidopsis leaves

Both malate and citrate are centrally positioned in the plant primary metabolism network and are found in the apoplast as well as in several cellular compartments, such as the cytosol, mitochondria, peroxisomes, glyoxysomes, chloroplasts, and vacuoles (3, 28, 29). The latter organelle can occupy up to 90% of the cell volume, making the vacuole responsible for dynamic storage of malate. Therefore, this organelle is of central importance for keeping the cytosolic malate homeostasis, a prerequisite for integrating all the pathways where this carboxylic acid is involved. Accordingly, we have to understand how import and export of malate across the vacuolar membrane is executed and regulated.

As reported earlier, a lack of tDT activity leads to a decrease in the malate uptake into *Arabidopsis* vacuoles as well as to decreased malate levels in the corresponding plant leaves (8). Along with these changes, an increase in total citrate concentration was observed in leaves from *tdt* knockout mutants (8, 21). However, the increase in citrate levels in these mutants could so far not be explained on the basis of the previously deciphered transport properties of tDT (8, 21).

The metabolic profiling of *tDT* overexpressor lines revealed that this change in tDT activity corresponds to significantly higher leaf malate contents as well as decreased citrate levels during an entire diurnal cycle and after the onset of drought stress, when compared with WT plants (Figs. 1 and 2). Because drought-induced malate accumulation and the accompanying citrate mobilization are absent in *tdt1* mutants, whereas this phenomenon is markedly pronounced in both *tdt* overexpressor lines (Fig. 2, *A* and *B*), we conclude that the tDT protein is responsible for reciprocal malate/citrate changes in *Arabidopsis* leaves. Interestingly, drought-induced malate accumulation

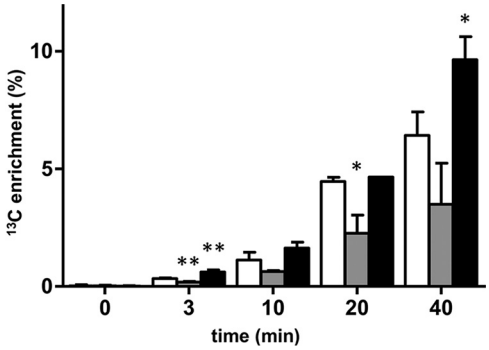

Figure 7. ^{13}C enrichment (percentage) in malate. Rosette leaves of WT (*white bars*), knockout (*gray bars*), and *tDT* overexpressor plants (*black bars*) were labeled with $^{13}CO_2$ for 0, 3, 10, 20, and 40 min. Each *data point* represents the mean value of three biological replicates ± S.D. (*error bars*). Due to technical difficulties, here are only two replicates for WT labeled for 20 min and one sample for the *tdt1* line labeled for 20 min. Significant differences from values obtained in WT according to Student's *t* test are indicated by *asterisks* (*, $p < 0.05$; **, $p < 0.01$).

is not limited to *Arabidopsis* but has also been observed in other species (30). Accordingly, the stimulatory effect of malate on *tdt* gene expression (14) is fully in line with the observed impact of altered tDT activity on malate accumulation (Fig. 2, *A* and *B*). Moreover, the observation that the malate/citrate ratios in leaves from *tDT* overexpressor mutants are always higher than in WT plants (Figs. 1 and 2) further supports the conclusion that tDT activity is a limiting factor for this reciprocal alteration of these carboxylate levels in wildtypes.

These conclusions also predict that low malate levels present in *tDT* knockout mutant leaves (Figs. 1 and 2) lead to a relative increase of cytosolic malate levels. Metabolite measurements in WT and *tdt1* knockout plants suggested that the absence of tDT leads to cytosolic malate accumulation (21, 23). Thus, the fact that the comparably low total malate pool in *tDT* knockout plants is labeled faster by newly assimilated $^{13}CO_2$ (Fig. 7) serves as an independent proof that *tdt1* mutants exhibit an accumulation of malate in the cytosol. Moreover, the observation that the large total malate pool in *tDT* overexpressor plants is labeled more slowly after administration of $^{13}CO_2$ (Fig. 7) independently supports the notion that tDT activity is a limiting factor for vacuolar malate accumulation. In addition, the correlation of a cold-induced increase of the malate concentration (31) with a concomitant increase of the tDT protein level (32) further points to a superior function of tDT for malate accumulation in leaves.

tDT exhibits an extended substrate spectrum and transports carboxylates in the dianion (2−) form

It has already been speculated that tDT is capable of both vacuolar import and export of malate (8, 21), although no transport mode of tDT has so far been put forward that would explain this phenomenon. Interestingly, neither the type of transport catalyzed by tDT nor its substrate spectrum has so far been analyzed in detail.

According to the data obtained in this study, we now have to extend the substrate spectrum of tDT by citrate because transmembrane movement of this tricarboxylate by tDT has been unequivocally documented on proteoliposomes harboring the functionally reconstituted tDT protein (Figs. 3 and 4). In addition to malate and citrate, tDT obviously accepts other carboxylates like succinate and fumarate, but not solutes such as sulfate, phosphate, or gluconate (Fig. 5). Thus, our documented fumarate transport activity by tDT (Fig. 5) is in line with the previous observation that leaves from *tdt* knockout plants exhibit not only decreased malate levels but also less fumarate (21). In fact, the ability of tDT to accept various carboxylates as transport molecules is reminiscent of the broad substrate specificity of the closest tDT homolog from mammalian cells, namely NaDC1 (33), which is involved in the sodium-energized reabsorption of a large number of Krebs cycle intermediates (34).

Whereas several members of the tDT homologs in animal systems, namely SLC13 proteins, also transport sulfate (16), we demonstrated that tDT from *Arabidopsis* does not accept sulfate or its structurally related phosphate as substrates (Fig. 5). This inability of tDT to accept sulfate and phosphate as substrates concurs, however, with the presence of specific PO_4^{2-} and SO_4^{2-} carriers in the vacuolar membrane (35, 36). It appears likely that the functions of the latter carriers in controlling cellular phosphate and sulfate homeostasis would be hampered by the simultaneous presence of additional carboxylate/SO_4^{2-} or carboxylate/PO_4^{2-} transport capacity across the tonoplast.

Changes in the medium pH affect both apparent substrate affinities and malate/citrate transport rates of tDT (Figs. 5 and 6 and Table 1). For an interpretation of these effects, we have to consider that the medium pH determines the relative abundance of various protonated forms of carboxylates (Fig. 6). Malate is mostly existent as a di-anion (malate^{2-}) at all tested pH values, having a majority of more than 90% at pH 6.2 (or even higher at pH 7.0 and 7.8; see CurTiPot under "Experimental procedures"). By contrast, the net charge of the citrate ion is strongly pH-dependent, and most of this tricarboxylate changes from the 3− to the 2− form, even in the pH range from 7.0 to 6.2 (see Fig. 6), a range similar to the pH gradient across the vacuolar membrane (2, 37). Interestingly, the highest citrate uptake was measured at pH 4.6, whereas further acidification to pH 4.0 provoked decreased citrate transport, presumably due to the formation of citrate^{1-} (Fig. 6). Accordingly, citrate^{2-} is probably the most efficient substrate for tDT. Because the cytosolic pH is situated around pH 7.5 and because the vacuole exhibits an acidic pH, it is tempting to assume that the so far unknown vacuolar citrate importer prefers the trivalent anionic form and that *in vivo* the major role of AttDT is to release citrate from the vacuole in exchange with another dicarboxylate, which at the cytosolic pH is present as dianions.

The electrophysiological studies on isolated vacuoles (Fig. S3) further support the assumption that tDT prefers divalent carboxylates as substrates. This conclusion is based on the fact that, although WT and overexpressor vacuoles exhibit tDT activity (8) (Figs. 1 and 2), no electrogenic malate-induced currents are detectable on isolated vacuoles (Fig. S3). Interestingly, the preference of tDT from *Arabidopsis* to accept carboxylates in the divalent anionic form concurs with the basic transport properties of the corresponding animal-specific protein SLC13 (15, 16, 33), being structurally the closest tDT-homologous transporter. Interestingly, whereas tDT transports its substrates in a counterexchange mode (Fig. 5), all other SLC13

members analyzed so far are characterized to be sodium/carboxylate symporters (15, 34). Both the pH dependence and the electrophysiological experiments indicate that citrate is transported in its dianionic form. Consequently, by exchanging carboxylates bearing two negative charges between the cytosol and the vacuole, the tDT protein acts as an electroneutral transporter. Experiments looking only at exchanges between malate and citrate would not exclude a directional transport (*e.g.* malate into and citrate out of the vacuole or vice versa), because the protein has been reconstituted in the 1:1 orientation. However, the fact that malate can be exchanged with malate and citrate can be exchanged with citrate (Fig. 3) indicates that there is not a specific substrate preference on one side of the transporter.

The counterexchange properties of tDT explain reciprocal malate/citrate changes in plant leaves

For the following reasons, we propose that tDT catalyzes a stoichiometric counterexchange of malate and citrate across the vacuolar membrane. First, *tDT* knockout and overexpressor mutants showed marked and always reciprocal concentration changes of malate and citrate in leaves (Figs. 1 and 2). Second, the proteoliposome system unequivocally demonstrated homo- and hetero-back-exchange of citrate and malate by tDT (Figs. 5 and 6 and Fig. S3). Third, malate/citrate exchange across tDT harboring proteoliposomes occurs in a nearly 1:1 stoichiometry (Fig. 5*A*, inset).

Whereas a homo-exchange of either malate against malate or citrate against citrate would not alter the cellular carboxylate homeostasis, any hetero-exchange would, however, influence the intracellular compartmentation of corresponding substrates. Given that tDT mediates a counterexchange of malate against citrate and citrate accumulates in the *tdt* mutant, we have to predict that increased vacuolar citrate concentrations in tDT knockout lines (Figs. 1 and 2) are due to the presence of other citrate-transporting proteins in the vacuolar membrane. In fact, for citrate, at least three different citrate import systems, which have so far not been identified at the molecular level, have been proposed comprising (i) a citrate-transporting anion channel (38), (ii) an ATP-dependent citrate transporter of unknown molecular identity (39), and (iii) a carrier protein, also of unknown molecular structure, accepting both di- and tricarboxylates as substrates (38, 40). Our results therefore suggest that citrate uptake into the vacuole is required, and it is the driving force for the uptake of other carboxylates, such as malate and fumarate.

Thus, the general ability of tDT to catalyze hetero-exchange of malate and citrate provokes now the question of the *in vivo* function of this carrier. Interestingly, similar to our findings on *Arabidopsis* (Fig. 1, *A* and *B*), diurnal reciprocal changes of malate and citrate levels have also been observed in tobacco leaves (41). Because malate is at the branching point of an impressive number of metabolic pathways and cellular reactions, such as amino acid biosynthesis, fatty acid biosynthesis, and metal and nutrient homeostasis (3, 29), the cytosolic malate concentrations in leaf cells are obviously well controlled and have been independently reported to be low at night and high during the day (42, 43). This typical diurnal pattern of malate and citrate recently even led to the development of a detailed metabolic "diel cycle" model, predicting that citrate has to be synthesized and stored in the night to serve as a carbon fuel for net amino acid synthesis, typically occurring in the next day phase (44).

However, accepting that malate and citrate are tightly coupled metabolites in the very active mitochondrial Krebs cycle (malate is the direct precursor for citrate synthesis), it is at first glance difficult to envisage how decreased malate levels can lead to increased citrate levels, and vice versa. This means that, although reciprocal changes of malate and citrate concentrations in leaves from higher plants have frequently been observed, no functional explanations for this phenomenon have so far been provided (45). However, due to the counterexchange capacity of tDT (Figs. 3–5 and Fig. S3), all reciprocal malate/citrate changes in leaves from higher plants can now be elegantly explained (*e.g.* in cases of increasing malate production during the day, this dicarboxylic acid enters the vacuole at the expense of luminal citrate, whereas in case of nocturnal malate consumption in the cytosol, citrate is imported).

The interpretation of metabolic change observed in mutants with modified mitochondrial enzyme activities led to the proposal that strict maintenance of certain cellular malate levels is critical for plant physiology and development (29, 46). However, *Arabidopsis tDT* mutants exhibit markedly modified malate and citrate concentrations (Figs. 1 and 2; see also Ref. 8) and, moreover, the corresponding changes in the relative cytosolic malate levels (Fig. 7; see also Ref. 21) without substantial phenotypic peculiarity, when compared with wildtypes. Obviously, apart from impaired regulation of the cytosolic pH-stat system in *tDT* knockout lines (21), *Arabidopsis* seems to be able to cope with these remarkable malate changes and might compensate for the lack of tDT by increased energy production, as indicated by stimulation of respiration in this mutant (21). Having now deciphered the transport properties of tDT in great detail, corresponding experiments, in which tDT mutants will be set under selected challenging conditions, can be optimized correspondingly.

Experimental procedures

Plant materials and growth conditions

Wildtype and transgenic *Arabidopsis* (*Arabidopsis thaliana*, ecotype Wassilewskija) plants were cultivated in a growth chamber on standard fertilized soil (ED-73) under short-day conditions (10-h light/14-h dark regime) at 21 °C and 125 μmol quanta m^{-2} s^{-1}. Light was provided by "B SERIES" LED lights (Valoya, Helsinki, Finland). For $^{13}CO_2$-labeling purpose, plants were grown in individual 6-cm diameter pots, with water/gas-permeable plastic foil (Aquafol®, Herrmann Meyer, Rellingen, Germany) between the rosette and the soil, in a growth chamber under short-day conditions (8-h light/16-h dark regime) at 22/20 °C day/night and 120 μmol quanta m^{-2} s^{-1}.

Loss-of-function mutants (*tdt1*) have already been described (8, 21). *At*tDT overexpressor lines (oex) were generated through the transformation of *tdt1* plants using the floral-dip method (47). Ten strong tDT overexpressor lines were identified via Northern blot analysis. oex lines 15 and 24 were further

characterized via quantitative real-time PCR. Drought stress was induced by subsequently withholding water for 14 days after the cultivation of plants for 3 weeks under standard conditions.

Northern blot analysis

Total RNA was isolated from frozen tissue samples using a Purescript® RNA extraction kit (Gentra Systems) according to the manufacturer's instructions. Determination of mRNA abundance was carried out as described previously (8).

Quantitative real-time PCR

RNA of the wildtype, *tdt1*, and the two overexpressor lines was extracted from frozen plant leaves using the NucleoSpin RNA plant kit (Macherey-Nagel, Düren, Germany), and the iScript cDNA synthesis kit (Bio-Rad, Munich, Germany) was used for cDNA synthesis according to the manufacturer's instructions. Quantitative real-time PCR was accomplished as described (48). Primers for the quantification of *At*tDT were *tDT-rt-fwd* (5′-ccgtcgaacactacaacatcc-3′) and *tDT-rt-rev* (5′-gctgttgtggcgcagatgc-3′). For transcript normalization, Ubiquitin10 (*At4g05320*) was used as a reference gene.

Ion chromatography–based quantification of carbonic acids

For isolation of carbonic acids, plant material was ground under liquid N_2, and 1 ml of double-distilled water was added to 100 mg, mixed thoroughly, and heated for 15 min at 95 °C. After centrifugation (15 min, 20,000 × *g*), the supernatant was used for ion chromatography quantification. For separation of soluble carbonic acids, a Metrosep-organic acid 250 column (Metrohm, Filderstadt, Germany), with 0.15 M H_2SO_4 as solvent, was used.

Recombinant synthesis, IMAC purification of tDT, and its functional reconstitution in proteoliposomes

E. coli BLR(DE3)pLysS cells (Merck Biosciences, Darmstadt, Germany) containing pET16b-*At*tDT were grown at 37 °C in Terrific Broth medium as described (49). At an A_{600} of 0.5–0.6, initiation of T7 RNA polymerase expression was induced by the addition of isopropyl-β-D-thiogalactopyranoside (1 mM). The cells were harvested 4 h postinduction by centrifugation (5,000 × *g*, 10 min, 20 °C), resuspended in buffer medium (1 mM EDTA, 15% glycerol, 10 mM Tris, pH 7.0), and immediately frozen in liquid N_2. To induce autolysis by the endogenous lysozyme, frozen cells were thawed at 37 °C and treated with a pinch of DNase and RNase. To avoid proteolytic activity, phenylmethanesulfonyl fluoride (1 mM) was added. Cell lysis was supported by sonication. During the first centrifugation step (20,000 × *g*, 15 min, 4 °C), cell debris were removed, and membranes were collected from the supernatant by centrifugation (100,000 × *g*, 30 min, 4 °C). Subsequent purification of tDT from these membranes was done at 4 °C. Membranes were resuspended in buffer medium B (10 mM NaCl, 5 mM imidazole, 50 mM Na_2HPO_4, pH 7.9) containing 0.5% DDM (Glycon Biomedicals) and stirred for 1 h to allow solubilization of intrinsic proteins. After centrifugation of the solubilized membranes (100,000 × *g*, 30 min, 4 °C), the supernatant was incubated for 2 h with Ni-NTA–agarose (Qiagen) to conduct IMAC.

The Ni-NTA suspension was transferred onto a chromatography column and washed with 10 volumes of the Ni-NTA–agarose bed volume with buffer medium B containing 0.5% DDM and then afterward with 6 column volumes of buffer medium W (10 mM NaCl, 60 mM imidazole, 50 mM Na_2HPO_4, pH 7.9, 0.5% DDM). Subsequently, recombinant tDT was eluted with an appropriate amount of buffer medium E (10 mM NaCl, 500 mM imidazole, 50 mM Na_2HPO_4, pH 7.9, 0.5% DDM) to obtain a protein concentration of 0.4–0.5 mg/ml.

Immediately after purification of tDT, 50 μl of the eluate was mixed with a homogeneous emulsion of 400 μl of L-α-phosphatidylcholine (125 mg/ml; type IV-S, Sigma) in buffer medium TG1 (100 mM Tricine, 30 mM potassium gluconate, pH 7.0). For loading, 50 μl of the indicated carbonic acids were added to achieve the indicated concentrations. After vigorous vortexing, the mixture (500 μl) was frozen in liquid N_2. Proteoliposomes were thawed on ice and sonified for 20 s (Sonifier 250, Branson) at the lowest output level and 50% duty cycle. Proteoliposomes (500 μl) were applied to a NAP-5 column (GE Healthcare) equilibrated with TG2 (10 mM Tricine, 150 mM potassium gluconate, pH 7.0) to remove external organic acids. Proteoliposomes were eluted from the column with 1 ml of TG2.

Malate and citrate uptake studies on proteoliposomes

100 μl of proteoliposomes were added to 100 μl of TG2 containing ^{14}C-labeled malate or citrate, respectively, at the indicated concentrations and pH values. For transport measurements, proteoliposomes were incubated at 30 °C, and uptake was terminated at the indicated time periods by removal of residual organic acids using anion-exchange chromatography (Dowex 1 × 8 Cl^-, 200–400-mesh) (50). Liposomes were eluted from the chromatography column by the addition of 1.5 ml of Tricine (200 mM, pH 7.0). Radioactivity in the eluate was quantified by scintillation counting (Canberra-Packard).

Analysis of the stoichiometry of malate/citrate transport across the proteoliposomal membrane

Proteoliposomes were loaded (see above) with 50 μl of ^{14}C-labeled or non-labeled malate (50 μM), respectively. Non-labeled citrate or ^{14}C-labeled citrate was added, and uptake of radiolabeled citrate was set against the release of radiolabeled malate.

Calculation of citrate and malate-ion distribution at different pH values

The calculation of the citrate ion and malate ion distribution at different pH values was done using the freeware CurTiPot analysis program (version 4.2; I. G. R. Gutz, University of Sao Paulo, Brazil).

$^{13}CO_2$-labeling studies

Labeling was performed on 5-week-old plants as described (27). The experiment was started 2 h after the onset of light, and the last labeled plant was harvested 1 h before the onset of darkness. Individual plants in their pot were quickly moved in the labeling chamber under the light field and quenched 0, 3, 10, 20, and 40 min after the start of labeling in a random manner

over the course of 2 days. Three biological replicates were obtained for each labeling condition (due to technical difficulties, here are only two replicates for WT labeled for 20 min and one sample for the *tdt1* line labeled for 20 min). Metabolism was quenched directly in the chamber by pouring a large volume of liquid N_2 over the rosette through a funnel. All frozen plant material above the plastic foil was collected and stored at −80 °C and then ground under liquid N_2. For LC-MS/MS quantification, metabolites were extracted from 15 mg (fresh weight) of frozen plant powder (27). Extracts were analyzed, and data were processed as described earlier (27).

Electrophysiological studies on isolated Arabidopsis vacuoles

For patch clamp, rosette leaves were digested in digest solution (10 mM MES, pH 5.3, adjusted with KOH, 1 mM $CaCl_2$, 500 mM sorbitol, 0.3% (w/v) cellulase "Onozuka R-10" (Serva, Heidelberg, Germany), 0.03% (w/v) pectolyase Y-23 (Kyowa Chemical Industry Co., Osaka, Japan) for 35 min at 30 °C. Protoplasts were lysed in standard bath solution (100 mM citric acid, pH-adjusted with BisTris propane to pH 7.5, osmotic content adjusted to 500 mosmol/kg with sorbitol) to release vacuoles. Borosilicate thin-wall capillaries were internally coated with Sigmacoat® (Sigma-Aldrich) and prepared to give a resistance of 3 ± 1 megaohms. Pipette tips were coated with silicone (Sylgard® 184 Silicone Elastomer Kit, Dow Corning, Wiesbaden, Germany) to reduce pipette capacitance. The pipette solution contained 100 mM citric acid, 10 mM HCl, 2 mM $CaCl_2$ and was adjusted with BisTris propane to pH 7.5, and the osmotic content was adjusted to 550 mosmol/kg with sorbitol. Pipettes were mounted onto a HEKA amplifier headstage connected to a HEKA EPC 10 USB amplifier (HEKA Elektronik Dr. Schulze GmbH, Lambrecht, Germany). The reference electrode was a 3 M KCl, 0.1% agarose bridge. Seals larger than 2 gigaohms were established, and upon break-in, the whole-vacuole configuration was established. The vacuolar lumen was allowed to equilibrate with the pipette solution for 5–10 min. Vacuoles were perfused with standard bath solution that contained either 100 mM citric acid or 100 mM malic acid. In all experiments, the measured liquid junction potential was below 1 mV, and therefore no correction was applied. The sampling interval was 1 kHz, and currents were filtered at 0.3 kHz (Patchmaster, HEKA).

Author contributions—B.F. and S.A. formal analysis; C.E., E.M., S.H., X.-Z.C., and S.A. methodology; E.M. data curation; X.-Z.C. and H.E.N. supervision; H.E.N. conceptualization; H.E.N. funding acquisition; H.E.N. writing-original draft.

Acknowledgments—We thank K. Awaad and S. Wic (University of Kaiserslautern) for help during generation of tDT overexpressor lines.

References

1. Neuhaus, H. E. (2007) Transport of primary metabolites across the plant vacuolar membrane. *FEBS Lett.* **581,** 2223–2226 CrossRef Medline
2. Hedrich, R. (2012) Ion channels in plants. *Physiol. Rev.* **92,** 1777–1811 CrossRef Medline
3. Fernie, A. R., and Martinoia, E. (2009) Malate. Jack of all trades or master of a few? *Phytochemistry* **70,** 828–832 CrossRef Medline
4. Clemens, S. (2006) Toxic metal accumulation, responses to exposure and mechanisms of tolerance in plants. *Biochimie* **88,** 1707–1719 CrossRef Medline
5. Raven, J. A. (1990) Sensing pH? *Plant Cell Physiol.* **13,** 721–729 CrossRef
6. Martinoia, E., and Rentsch, D. (1994) Malate compartmentation: responses to a complex metabolism. *Annu. Rev. Plant Physiol. Plant Mol. Biol.* **45,** 447–467 CrossRef
7. Martinoia, E., Maeshima, M., and Neuhaus, H. E. (2007) Vacuolar transporters and their essential role in plant metabolism. *J. Exp. Bot.* **58,** 83–102 Medline
8. Emmerlich, V., Linka, N., Reinhold, T., Hurth, M. A., Traub, M., Martinoia, E., and Neuhaus, H. E. (2003) The plant homolog to the human sodium/dicarboxylic cotransporter is the vacuolar malate carrier. *Proc. Natl. Acad. Sci. U.S.A.* **100,** 11122–11126 CrossRef Medline
9. Cerana, R., Giromini, L., and Colombo, R. (1995) Malate-regulated channels permeable to anions in vacuoles of *Arabidopsis thaliana*. *Aust. J. Plant Physiol.* **22,** 115–121 CrossRef
10. Iwasaki, I., Arata, H., Kijima, H., and Nishimura, M. (1992) Two types of channels involved in the malate ion transport across the tonoplast of a crassulacean acid metabolism plant. *Plant Physiol.* **98,** 1494–1497 CrossRef Medline
11. Kovermann, P., Meyer, S., Hörtensteiner, S., Picco, C., Scholz-Starke, J., Ravera, S., Lee, Y., and Martinoia, E. (2007) The *Arabidopsis* vacuolar malate channel is a member of the ALMT family. *Plant J.* **52,** 1169–1180 CrossRef Medline
12. Cheffings, C. M., Pantoja, O., Ashcroft, F. M., and Smith, J. A. C. (1997) Malate transport and vacuolar ion channels in CAM plants. *J. Exp. Bot.* **48,** 623–631 CrossRef Medline
13. Pantoja, O., and Smith, J. A. C. (2002) Sensitivity of the plant vacuolar malate channel to pH, Ca^{2+} and anion-channel blockers. *J. Membr. Biol.* **186,** 31–42 CrossRef Medline
14. Hafke, J. B., Hafke, Y., Smith, J. A. C., Lüttge, U., and Thiel, G. (2003) Vacuolar malate uptake is mediated by an anion-selective inward rectifier. *Plant J.* **35,** 116–128 CrossRef Medline
15. Pajor, A. M. (2006) Molecular properties of the SLC13 family of dicaboxylate and sulfate transporters. *Pflugers Arch.* **451,** 597–605 CrossRef Medline
16. Bergeron, M. J., Clémençon, B., Hediger, M. A., and Markovich, D. (2013) SLC13 family of Na^+-coupled di- and tri-carboxylate/sulfate transporters. *Mol. Aspects Med.* **34,** 299–312 CrossRef Medline
17. Ye, J., Wang, X., Hu, T., Zhang, F., Wang, B., Li, C., Yang, T., Li, H., Lu, Y., Giovannoni, J. J., Zhang, Y., and Ye, Z. (2017) An InDel in the promoter of Al-activated malate transporter 9 selected during tomato domestication determines fruit malate contents and aluminum tolerance. *Plant Cell* **29,** 2249–2268 CrossRef Medline
18. Delhaize, E., Ryan, P. R., Hebb, D. M., Yamamoto, Y., Sasaki, T., and Matsumoto, H. (2004) Engineering high-level aluminum tolerance in barley with the ALMT1 gene. *Proc. Natl. Acad. Sci. U.S.A.* **101,** 15249–15254 CrossRef Medline
19. De Angeli, A., Zhang, J., Meyer, S., and Martinoia, E. (2013) AtALMT9 is a malate-activated vacuolar chloride channel required for stomatal opening in *Arabidopsis*. *Nat. Commun.* **4,** 1804 CrossRef Medline
20. Baetz, U., Eisenach, C., Tohge, T., Martinoia, E., and De Angeli, A. (2016) Vacuolar chloride fluxes impact ion content and distribution during early salinity stress. *Plant Physiol.* **172,** 1167–1181 Medline
21. Hurth, M. A., Suh, S. J., Kretzschmar, T., Geis, T., Bregante, M., Gambale, F., Martinoia, E., and Neuhaus, H. E. (2005) Impaired pH homeostasis in *Arabidopsis*, lacking the vacuolar dicarboxylate transporter and analysis of carboxylic acid transport across the tonoplast. *Plant Physiol.* **137,** 901–910 CrossRef Medline
22. Liu, R., Li, B., Qin, G., Zhang, Z., and Tian, S. (2017) Identification and functional characterization of a tonoplast dicarboxylate transporter in tomato (*Solanum lycopersicum*). *Front. Plant Sci.* **8,** 186 Medline
23. Medeiros, D. B., Barros, K. A., Barros, J. A. S., Omena-Garcia, R. P., Arrivault, S., Sanglard, L. M. V. P., Detmann, K. C., Silva, W. B., Daloso, D. M., DaMatta, F. M., Nunes-Nesi, A., Fernie, A. R., and Araújo, W. L. (2017) Impaired malate and fumarate accumulation due the mutation of tono-

plast dicarboxylate transporter. *Plant Physiol.* **175,** 1068–1081 CrossRef Medline
24. Krasensky, J., and Jonak, C. (2012) Drought, salt, and temperature stress-induced metabolic rearrangements and regulatory networks. *J. Exp. Bot.* **63,** 1593–1608 CrossRef Medline
25. Oxender, D. L. (1972) Amino acid transport in microorganisms. In *Metabolic Transport*, 3rd Ed. (Hokin, L., ed) pp. 133–185, Academic Press, Inc., New York
26. Trentmann, O., Jung, B., Neuhaus, H. E., and Haferkamp, I. (2008) Non-mitochondrial ATP/ADP transporters accept phosphate as third substrate. *J. Biol. Chem.* **283,** 36486–36493 CrossRef Medline
27. Szecowka, M., Heise, R., Tohge, T., Nunes-Nesi, A., Vosloh, D., Huege, J., Feil, R., Lunn, J., Nikoloski, Z., Stitt, M., Fernie, A. R., and Arrivault, S. (2013) Metabolic fluxes in an illuminated *Arabidopsis* rosette. *Plant Cell* **25,** 694–714 CrossRef Medline
28. Popova, T. N., and Pinheiro de Carvalho, M. A. (1998) Citrate and isocitrate in plant metabolism. *Biochim. Biophys. Acta* **1364,** 307–325 CrossRef Medline
29. Finkemeier, I., and Sweetlove, L. J. (2009) The role of malate in plant homeostasis. *F1000 Biol. Rep.* **1,** 47 Medline
30. Cramer, G. R., Ergül, A., Grimplet, J., Tillett, R. L., Tattersall, E. A. R., Bohlman, M. C., Vincent, D., Sonderegger, J., Evans, J., Osborne, C., Quilici, D., Schlauch, K. A., Schooley, D. A., and Cushman, J. C. (2007) Water and salinity stress in grapevines: early and late changes in transcript and metabolite profiles. *Funct. Integr. Genomics* **7,** 111–134 CrossRef Medline
31. Cook, D., Fowler, S., Fiehn, O., and Thomashow, M. F. (2004) A prominent role for the CBF cold response pathway in configuring the low-temperature metabolome of *Arabidopsis*. *Proc. Natl. Acad. Sci. U.S.A.* **101,** 15243–15248 CrossRef Medline
32. Schulze, W. X., Schneider, T., Starck, S., Martinoia, E., and Trentmann, O. (2012) Cold acclimation induces changes in *Arabidopsis* tonoplast protein abundance and activity and alters phosphorylation of tonoplast monosaccharide transporters. *Plant J.* **69,** 529–541 CrossRef Medline
33. Yao, X., and Pajor, A. M. (2000) The transport properties of the human renal Na^+- dicarboxylate cotransporter under voltage-clamp conditions. *Am. J. Physiol. Renal Physiol.* **279,** F54–F64 CrossRef Medline
34. Pajor, A. M. (1999) Sodium-coupled transporters for Krebs cycle intermediates. *Annu. Rev. Physiol.* **61,** 663–682 CrossRef Medline
35. Kataoka, T., Watanabe-Takahashi, A., Hayashi, N., Ohnishi, M., Mimura, T., Buchner, P., Hawkesford, M. J., Yamaya, T., and Takahashi, H. (2004) Vacuolar sulfate transporters are essential determinants controlling internal distribution of sulfate in *Arabidopsis*. *Plant Cell* **16,** 2693–2704 CrossRef Medline
36. Liu, J., Yang, L., Luan, M., Wang, Y., Zhang, C., Zhang, B., Shi, J., Zhao, F. G., Lan, W., and Luan, S. (2015) A vacuolar phosphate transporter essential for phosphate homeostasis in *Arabidopsis*. *Proc. Natl. Acad. Sci. U.S.A.* **112,** E6571–E6578 CrossRef Medline
37. Rienmüller, F., Dreyer, I., Schönknecht, G., Schulz, A., Schumacher, K., Nagy, R., Martinoia, E., Marten, I., and Hedrich, R. (2012) Luminal and cytosolic pH feedback on proton pump activity and ATP affinity of V-type ATPase from *Arabidopsis*. *J. Biol. Chem.* **287,** 8986–8993 CrossRef Medline
38. White, P. J., and Smith, J. A. C. (1989) Proton and anion transport at the tonoplast in crassulacean-acid-metabolism plants: specificity of the malate-influx system in *Kalanchoë daigremontiana*. *Planta* **179,** 265–274 CrossRef Medline
39. Canel, C., Bailey-Serres, J. N., and Roose, M. L. (1996) Molecular characterization of the mitochondrial citrate synthase gene of an acidless pummelo (*Citrus maxima*). *Plant Mol. Biol.* **31,** 143–147 CrossRef Medline
40. Rentsch, D., and Martinoia, E. (1991) Citrate transport into barley mesophyll vacuoles: comparison with malate uptake activity. *Planta* **184,** 532–537 Medline
41. Scheible, W. R., Krapp, A., and Stitt, M. (2000) Reciprocal diurnal changes of phosphoenolpyruvate carboxylase expression and cytosolic pyruvate kinase, citrate synthase and NADP-isocitrate dehydrogenase expression regulate organic acid metabolism during nitrate assimilation in tobacco leaves. *Plant Cell Environ.* **23,** 1155–1167 CrossRef
42. Gerhardt, R., Stitt, M., and Heldt, H. W. (1987) Subcellular metabolite levels in spinach leaves: regulation of sucrose synthesis during diurnal alterations in photosynthesis. *Plant Physiol.* **83,** 399–407 CrossRef Medline
43. Chang, K., and Roberts, J. K. M. (1991) Cytoplasmic malate levels in maize root tips during K^+ ion uptake determined by ^{13}C-NMR spectroscopy. *Biochim. Biophys. Acta* **1092,** 29–34 CrossRef Medline
44. Cheung, C. Y., Poolman, M. G., Fell, D. A., Ratcliffe, R. G., and Sweetlove, L. J. (2014) A diel flux balance model captures interactions between light and dark metabolism during day-night cycles in C3 and crassulacean acid metabolism leaves. *Plant Physiol.* **165,** 917–929 CrossRef Medline
45. Igamberdiev, A. U., and Eprintsev, A. T. (2016) Organic acids: the pools of fixed carbon involved in redox regulation and energy balance in higher plants. *Front. Plant Sci.* **7,** 1042 Medline
46. Fernie, A. R., Carrari, F., and Sweetlove, L. J. (2004) Respiratory metabolism: glycolysis, the TCA cycle and mitochondrial electron transport. *Curr. Opin. Plant Biol.* **7,** 254–261 CrossRef Medline
47. Clough, S. J., and Bent, A. F. (1998) Floral dip: a simplified method for *Agrobacterium*-mediated transformation of *Arabidopsis thaliana*. *Plant J.* **16,** 735–743 CrossRef Medline
48. Wormit, A., Trentmann, O., Feifer, I., Lohr, C., Tjaden, J., Meyer, S., Schmidt, U., Martinoia, E., and Neuhaus, H. E. (2006) Molecular identification and physiological characterization of a novel monosaccharide transporter from *Arabidopsis* involved in vacuolar sugar transport. *Plant Cell* **18,** 3476–3490 CrossRef Medline
49. Haferkamp, I., Hackstein, J. H., Voncken, F. G., Schmit, G., and Tjaden, J. (2002) Functional integration of mitochondrial and hydrogenosomal ADP/ATP carriers in the *Escherichia coli* membrane reveals different biochemical characteristics for plants, mammals and anaerobic chytrids. *Eur. J. Biochem.* **269,** 3172–3181 CrossRef Medline
50. Krämer, R., and Klingenberg, M. (1980) Modulation of the reconstituted adenine nucleotide exchange by membrane potential. *Biochemistry* **19,** 556–560 CrossRef Medline